Carbohydrate Polymers 95 (2013) 434–440

Contents lists available at SciVerse ScienceDirect

Carbohydrate Polymers

journal homepage: www.elsevier.com/locate/carbpol

Cellulose acetate–zirconium (IV) phosphate nano-composite with enhanced photo-catalytic activity

Vinod Kumar Gupta[a,b,*], Deepak Pathania[c], Pardeep Singh[c], Bhim Singh Rathore[c], Priyanka Chauhan[c]

[a] Department of Chemistry, Indian Institute of Technology Rookree, Roorkee 247667, India
[b] Chemistry Department, King Fahd University of Petroleum & Minerals, Dhahran 31261, Saudi Arabia
[c] Department of Chemistry, Shoolini University, Solan 173212, Himachal Pradesh, India

ARTICLE INFO

Article history:
Received 11 January 2013
Received in revised form 7 February 2013
Accepted 21 February 2013
Available online 4 March 2013

Keywords:
Cellulose acetate
Zirconium (IV) phosphate
Nanocomposite
Ion exchange property
Photocatalysis

ABSTRACT

Cellulose acetate–zirconium (IV) phosphate nanocomposite (CA/ZPNC) was synthesized by sol–gel technique at pH 0–1 and was characterized by X-ray diffraction (XRD), scanning electron microscopy (SEM), energy dispersive X-ray (EDX) spectroscopy, Fourier infrared spectroscopy (FTIR) and thermal analysis (TGA/DTA/DSC). Ion exchange capacity, pH titration, elution concentration, elution behaviour, thermal stability and distribution coefficient were investigated to explore ion exchange behaviour of CA/ZPNC. The nanocomposite showed an ion-exchange capacity of 1.4 mequiv. g^{-1} for Na^+ and was highly selective for Pb^{2+} and Zn^{2+} over many other metal ions. The photocatalytic activity of the CA/ZPNC was explored for degradation of a model Congo red dye from aqueous phase. 90% of dye was removed in 60 min of irradiation. Simultaneous adsorption and photocatalysis had synergetic effect on dye degradation.

1. Introduction

Several industries such as textile, paper, paint, and dyestuffs consume large quantity of water and utilize chemicals and dyes to form products; as a consequence, several toxic metals and chemicals are discharged continuously into the water bodies. The discharged industrial pollutants deteriorate the water quality and may cause adverse effect on human health due to their toxic, mutagenic and carcinogenic nature (Gupta, Rastogi, & Nayak, 2010; Huang & Chen, 2009; Korbahti, Artut, Gecgel, & Ozer, 2011; Zhao et al., 2012). Congo red – an anionic dye has been known to cause an allergic reaction and is known to be metabolized to benzidine which in turn is a human carcinogen (Chatterjee, Lee, Lee, & Woo, 2009).

Wastewaters containing synthetic dyes and toxic metal ions are difficult to treat, since they are recalcitrant, resistant to biological oxidation/reduction, and are stable to oxidizing agents. The conventional methods such as coagulation, flocculation, precipitation, membrane separation, solvent extraction, adsorption and reverse osmosis are not able to treat industrial effluent effectively (Vilhera, Goncalves, & Mota, 2004). In practice, no single process provides adequate treatment and a combination of different processes is often used to improve the water quality in a greener and more economic way.

It is now well documented that low cost bio-adsorbent based adsorption processes are effective and economic methods for wastewater remediation (Gupta, Ali, & Saini, 2007; Gupta, Jain, & Varshney, 2007; Gupta, Agarwal, & Saleh, 2011; Gupta, Mittal, Malviya, & Mittal, 2009; Jain, Gupta, Bhatnagar, & Suhas, 2003; Mittal, Mittal, Malviya, & Gupta, 2009; Mittal, Mittal, Malviya, & Gupta, 2010; Mittal, Gupta, Malviya, & Mittal, 2008; Mittal, Mittal, Malviya, Kaur, & Gupta, 2010; Gupta, Gupta, Rastogi, Nayak, & Agarwal, 2011). A large variety of non-conventional bio-adsorbents have been employed to remove metal ions and dyes from aqueous phase. Much attention has been focused on fungal or bacterial biomass and biopolymers that are harmless and are ubiquitously available in nature (Constantin et al., 2013; Gupta et al., 2010; Oei, Ibrahim, Wang, & Ang, 2009; Yang et al., 2012). However, lack of stability, intricacies in separation from aqueous phase and low recovery after desorption are the major limitations for large scale application of bio-absorbents (Gupta et al., 2010).

In order to meet the stringent environmental regulation, the photocatalytic reactions have advantages over classical and non-conventional methods for dye degradation due to their simplicity and rapid degradation based on hydroxyl radical formation. Nowadays, hybrid organic–inorganic nanocomposites are materials of choice because of their multifunctionality due to a combination of different compounds incorporated. Recent examples can be found in the range of TiO_2, BiOCl, Fe_2O_3, CuS and ZnO based

* Corresponding author at: Department of Chemistry, Indian Institute of Technology Rookree, Roorkee 247667, India. Tel.: +91 1332285801; fax: +91 1332286202.
E-mail addresses: vinodfcy@gmail.com, vinodfcy@iitr.ernet.in (V.K. Gupta).

0144-8617/$ – see front matter © 2013 Elsevier Ltd. All rights reserved.
http://dx.doi.org/10.1016/j.carbpol.2013.02.045

nanocomposites (Dong, Sun, Min, Wu, & Lee, 2012; Liu, Sun, Liu, & Wang, 2013; Virkutyte, Jegatheesan, & Varma, 2012). Primarily, adsorption of pollutants on the catalyst surface is a pre-requisite for the effective photo-degradation process (Qourzal, Tamimi, Assabbane, & Ait-Ichou, 2005). However, little work has been done to develop hybrid nano-bio-composite material with high adsorption capacity and enhanced photocatalytic activity (Gupta, Ali, Saleh, Nayak, & Agarwal, 2012).

Recently, cellulose based nanocomposites have drawn considerable attention because of their low cost, high-volume application, easy processability, renewable nature and possibility of recycling (Ali, 2012). There are several research efforts reporting the cellulose composite with carbon nanotubes, lignin and lumiscent CdS (Nevarez et al., 2011; Park & Kadla, 2012; Yang et al., 2012). Fitz-Binder and Bechtold (2012) investigated the adsorption of Ca^{2+} ions on regenerated cellulose fibres such as lyocell, viscous and model fibres. Zirconium phosphate is an inorganic ion exchanger of the class of tetravalent metal acid (TMA) salts. It has been recently demonstrated as an excellent sorbent for heavy metals due to its high selectivity, high thermal stability and absolute insolubility in water. Thakkar and Chudasama (2009) studied the exchange properties of zirconium titanium phosphate (ZTP) for the separation of Cu^{2+}, Ni^{2+}, Zn^{2+}, Co^{2+}, Cd^{2+}, Hg^{2+}, Pb^{2+}, Bi^{2+}, La^{3+}, Ce^{2+}, Th^{4+}, and $UO_2{}^{2+}$. Kubli et al. (2012) synthesized zirconium phosphate based microporous ion exchanger that can discriminate between CO_2 and CH_4. Mishima, Matsuda, and Miyake (2007) studied the photocatalytic efficacy of Zr_2ON_2 yielding H_2 and O_2 by water reduction. However major disadvantage of synthetic inorganic ion exchangers is the difficulty in preparing granulated materials with sufficient strength and suitable mechanical properties for column operations.

Until now, as far as, we could ascertain, no data is available concerning the preparation of cellulose acetate–zirconium (IV) phosphate nanocomposite as a visible light active photocatalyst. The objective of the present work is to prepare cellulose acetate–zirconium (IV) phosphate nanocomposite (CA/ZPNC) by sol–gel transformations. The ion exchange behaviour of CA/ZPNC will be explored for the adsorption of different metal ions. The photocatalytic activity of CA/ZPNC was also utilized for the degradation of Congo red (CR) dye. It was characterized by scanning electron transmission (SEM), transmission electron microscopy (TEM), energy dispersive X-ray (EDX), thermo gravimetric and differential temperature analysis, X-ray diffraction (XRD) and Fourier transform infrared (FTIR) and ultraviolet–visible (UV–Vis) spectroscopy and subjected to ion-exchanger photocatalytic activity study.

2. Experimental

2.1. Chemicals and materials

The main reagents used were zirconium oxychloride, orthophosphoric acid, cellulose acetate and were purchased from Sigma–Aldrich, India. All reagents were used without further purification. The Congo red dye was obtained from S.D. Fine India. All other chemicals and reagents used were of analytical reagent grade. All the solutions were prepared in double distilled water.

2.2. Preparation of cellulose acetate Zirconium (IV) phosphate (CA/ZPNC)

In the present work, cellulose acetate based nanocomposite was synthesized using simple and ambient sol gel method (Fig. 1). Firstly, solutions of 0.1 M orthophosphoric acid and 0.1 M zirconium (IV) oxychloride were gradually mixed with continuous stirring at pH 2. After complete addition, the mixture was stirred for 30 min to obtain zirconium (IV) phosphate (ZP) precipitates. In the next step, cellulose acetate (CA) gel was prepared in concentrated formic acid and added to zirconium (IV) phosphate solution with continuous stirring for 4 h The resultant mixture was allowed to stand for 24 h with occasional shaking in the mother liquor for digestion. The precipitates were separated by filtration and washed with demineralised water several times to remove excess of the reagents. The precipitates were equilibrated with 0.1 M HNO_3 solution for 24 h to convert into H^+ form. It was then filtered and washed with demineralised water to remove any excess acid and finally dried in an oven at 80 °C.

2.3. Instrumentation

Thermal analysis of CA/ZPNC was performed on thermo gravimetric analyzer (NETZSCH TG 209 F1). X-ray diffraction data were recorded using X-ray diffractometer (Phillips, Holland, model PW 1148/89). Fourier transformer infrared (FTIR) spectra were obtained using Perkin Elmer spectrometer (Spectrum 400, USA). The surface morphology of the nanocomposite was studied using scanning electron microscope (SEM Quant-250, model 9393). The microstructure was analyzed by transmission electron microscopy (TEM) using Tecnai 20 G2 (Plate/CCD Camera). The concentration of dye was determined using Systronics 117UV–visible spectrophotometer.

2.4. Ion exchange activity of CA/ZPNC

2.4.1. Ion exchange capacity

The ion exchange capacity of CA/ZPNC was determined by standard column method. In this process, 0.5 g (dry mass) of CA/ZPNC in H^+ form was placed in a glass tube of 1 cm internal diameter at glass wool supported at the bottom. The column containing CA/ZPNC was washed with double distilled water to remove excess acid. 0.1 M NaCl (250 mL) solution was used to elute H^+ from the CA/ZPNC. The flow rate of eluent was maintained at 0.5 mL min^{-1}. The collected effluent was titrated against a standard alkali solution. The hydrogen ions released were calculated using the formula as discussed earlier (Siddiqui & Khan, 2007):

$$\text{IEC} = \frac{N \times V}{W} \text{mg/g} \quad (1)$$

where IEC is ion exchange capacity. N and V (mL) are normality and volume of NaOH, respectively. W (mg) is the amount of CA/ZPNC.Thermal stability

0.5 g sample of CA/ZPNC in H^+ form was heated at different temperatures in muffle furnace for 1 h. The sample was weighed and ion exchange capacity was determined after cooling to room temperature.

2.4.2. Effect of eluent concentration

The optimum concentration for complete elution of H^+ ions from CA/ZPNC was studied. 250 mL of $NaNO_3$ solution of different concentration was passed through the columns, containing 0.5 g of the exchanger in H^+ form with a flow rate of 0.5 mL min^{-1}. The collected eluents were titrated against 0.1 M NaOH in order to determine the eluted H^+ ions.

2.4.3. Elution behaviour

$NaNO_3$ solution (1 M) was passed through a column containing 0.5 g of CA/ZPNC for complete elution of H^+. Effluent was collected in 10 mL fraction at a flow rate of 0.5 mL min^{-1}. Each fraction of 10.0 mL was titrated with 0.1 M NaOH solution.

2.4.4. pH-titration

pH-titration studies were performed using Topp and Pepper method (Gupta, Pathania, Agarwal, & Singh, 2012). In typical

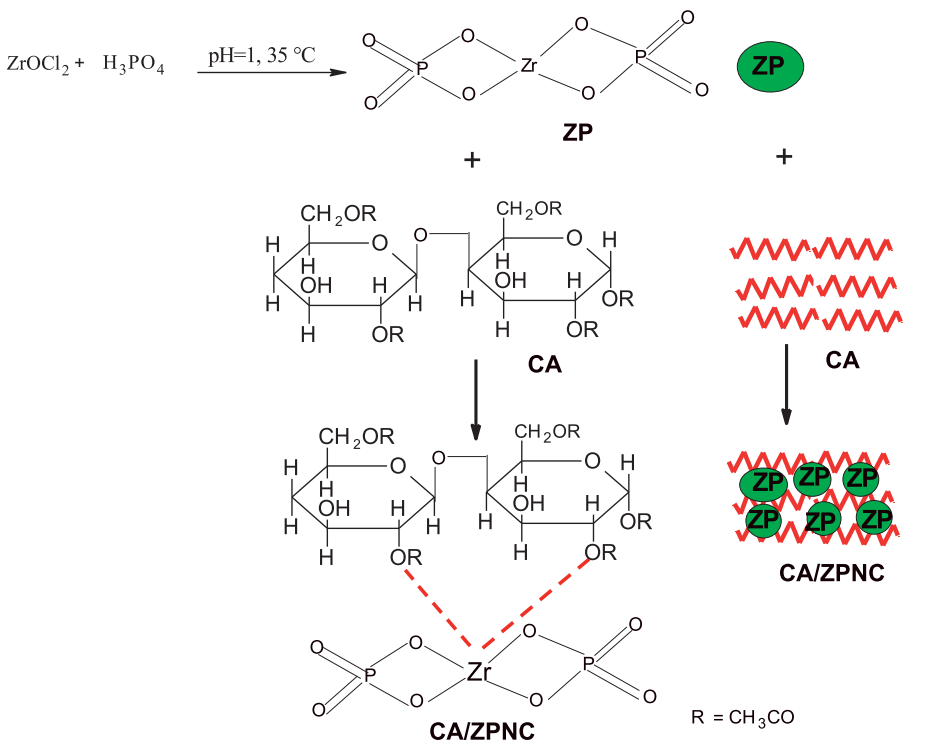

Fig. 1. Schematic diagram of preparation of cellulose acetate–zirconium acetate nanocomposite.

method, 0.5 g of CA/ZPNC in H^+ form was placed in each of 250 mL conical flasks containing equimolar solutions of alkali metal chlorides and their hydroxide in different volume ratios. Total volume was kept at 50 mL to make the ionic strength constant. pH of the solution was recorded every 24 h until equilibrium was attained in 10 days.

2.4.5. Distribution studies

Distribution coefficients of different metal ions such as Pb^{2+}, Zn^{2+}, Th^{2+}, Cu^{2+}, Ni^{2+}, Cd^{2+}, Mg^{2+} were determined in aqueous solution using batch process. 0.5 g of CA/ZPNC in H^+ form and 20 mL of different metal nitrate solutions were continuously shaken for 24 h at 25 °C. Metal ion concentration was determined by titrating against EDTA solution. K_d values (mL/g) were determined using following formula (Inamuddin, Khan, Siddiqui, & Khan, 2007; Siddiqui & Khan, 2007):

$$K_d = \frac{I - F}{F} \times \frac{V}{M} \quad (2)$$

where I and F indicate initial and final concentration of metal ion in solution. V and M denotes final volume of the solution (mL) and amount of ion exchanger (g), respectively.Photocatalytic and adsorption experiment

The photocatalytic experiment was carried out in a slurry type batch reactor (Gupta et al., 2012a). Double walled pyrex vessel was surrounded by thermostatic water circulation arrangement to keep temperature in the range of 30 ± 0.3 °C. During adsorption experiments, slurry composed of dye solution and CA/ZPNC (S-1) suspension was stirred magnetically and placed in dark to attain equilibrium. In case of photocatalytic studies, suspension composed of dye and catalyst was stirred for 10 min. Then suspension was exposed to natural solar light (solar intensity = 56 × 10^4 ± 250 lx) with continuous stirring. At specific time intervals, aliquot (3 mL) was withdrawn and centrifuged for 2 min to remove catalyst particles form aliquot. The dye concentration was determined at 490 nm spectrophotometrically. The decolourisation efficiency of dye was calculated using following equation:

$$\%\text{removal efficiency} = \frac{C_0 - C_t}{C_0} \times 100 \quad (3)$$

where C_0 is the initial and C_t is instant concentration of Congo red.

The kinetics of dye degradation was described by pseudo first order kinetics. The rate constant (k_{obs}) was calculated using the following equation:

$$k_{obs} = 2.303 \times \text{slope} \quad (4)$$

where the slope was obtained from the plot of ln(c) versus t.

3. Results and discussion

3.1. Characterization of CA/ZPNC

Scanning electron microscopy (SEM) images of CA/ZPNC at different magnifications are shown in Fig. 2(a and b) which exhibits rough surface with different sized particles to form microsphere. As seen in Fig. 2(c and d), TEM images signify homogeneous distribution of CA and ZP particles in nanocomposite. The darker portion represents CA wrapped in ZP while the grey part corresponds to CA in polymeric backbone. These images clearly indicate CA/ZPNC formation in the range of 50 nm.

Fig. 3(a) represents X-ray diffraction pattern of CA, ZP and CA/ZPNC. The broader diffraction peaks between 10° and 23° clearly indicates the amorphous nature of CA. The small intensity diffraction peaks near 20° are the characteristic peaks of ZP (Liu, Ma, Gan, Li, & Wang, 2012; Jo, Shin, & Wang, 2011). In case of ZPNC, emergence of low intensity broader peaks of ZP indicates the amorphous nature of nanocomposite.

EDX studies of CA/ZPNC are shown in Fig. 3(b). Zr, P, C and O elements are present in weight percentage of 30.27, 13.51, 12.55 and 43.67, respectively.

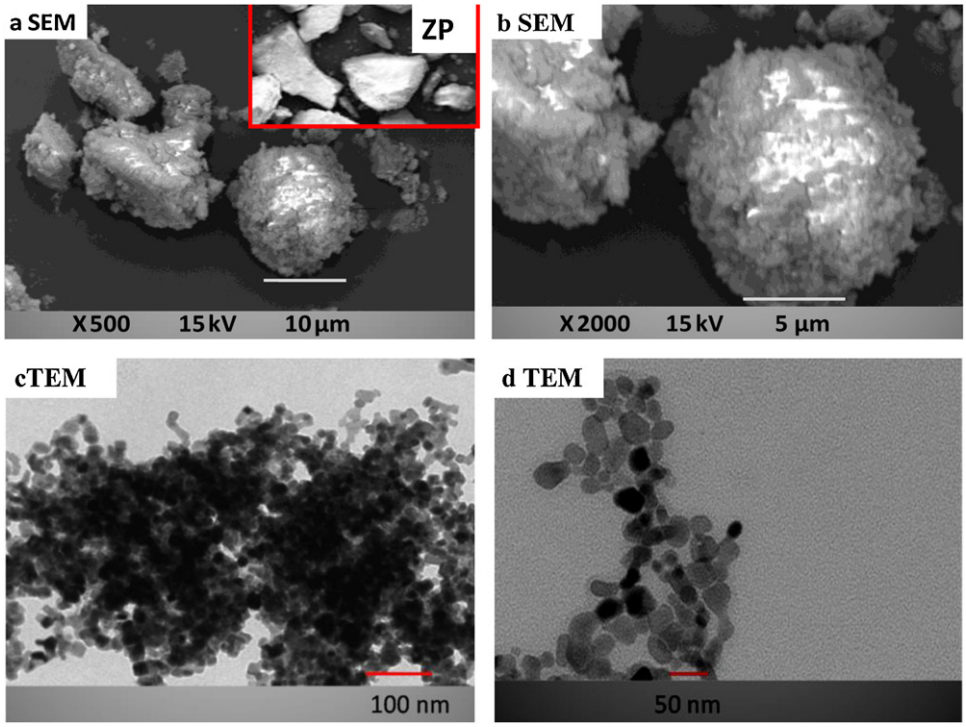

Fig. 2. SEM and TEM images of CA/ZPNC. Inset is SEM image of ZP.

FTIR spectrum of CA/ZPNC (Fig. 3(c)) shows a broad peak at 3423 cm^{-1} which may be assigned to water molecule. A sharp peak at 1631 cm^{-1} represents free water molecule (water of crystallization) and strongly bonded —OH group in the matrix. The peak at 1039 cm^{-1} may be due to occurrence of PO_4^{3-}, HPO_4^{2-} and $H_2PO_4^-$ (Siddiqui & Khan, 2007). Absorption band at 1734 cm^{-1}, corresponds to the carbonyl of ester group in cellulose acetate. The peaks at 520 and 610 cm^{-1} are due to the superposition of metal–oxygen stretching vibrations confirming binding between cellulose acetate and Zr (IV) phosphate. A sharp peak at 1389 cm^{-1} is assigned to hydroxyl groups vibration (Siddiqui & Khan, 2007).

It is seen from TGA curve (Fig. 4) that the initial loss of 16.7% (150.3 °C) is due to the removal of water from the nanocomposite (Inamuddin et al., 2007). Slow weight loss (11.7%) between 150 and 390 °C depicts condensation of phosphate group to pyrophosphate groups. Further weight loss up to 600 °C indicates complete decomposition of the organic part of the material. DTA curve illustrates small exothermic peaks at 53 °C, 103 °C, 215 °C, 451 °C and 550 °C confirming structural transformation in CA/ZPNC (Inamuddin et al., 2007; Siddiqui & Khan, 2007).

3.2. Ion exchange behaviour of CA/ZPNC

Different samples of new and novel organic-inorganic nanocomposite were prepared by the sol–gel mixing of inorganic matrices of Zr (IV) phosphate and cellulose acetate in different ratios (Table 1).

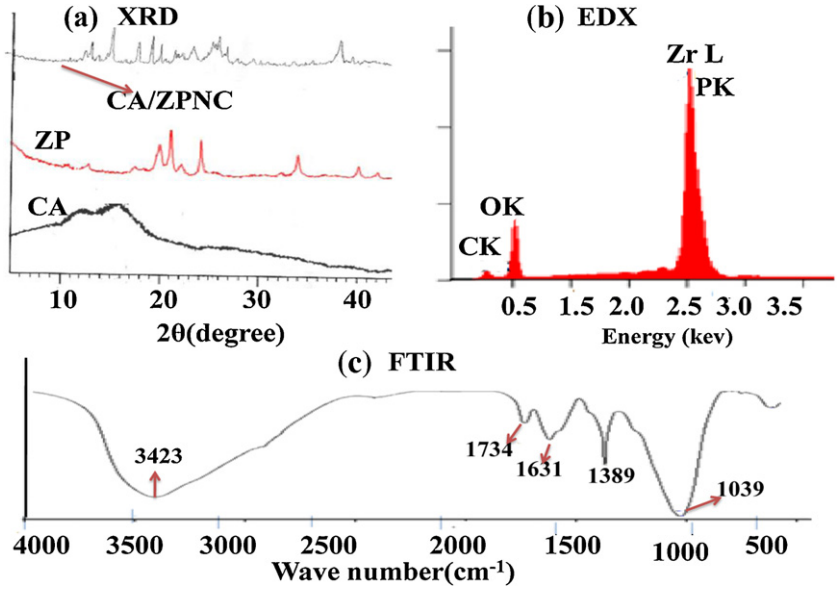

Fig. 3. XRD, EDX and FTIR spectra of CA/ZPNC.

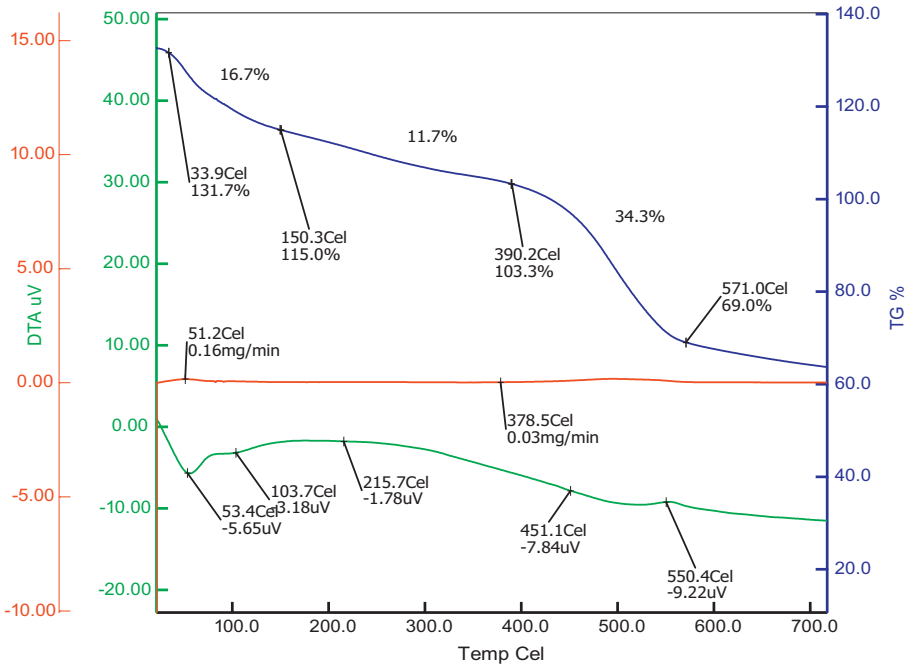

Fig. 4. TGA and DTA curves of CA/ZPNC.

Sample S-1 of CA/ZPNC possessed a better Na^+ ion-exchange capacity (1.4 mequiv. g^{-1}) as compared to their inorganic counterpart (sample S-5) (0.5 mequiv. g^{-1}) and was thus used in the further studies of characterization and testing. The improvement in the exchange capacity of nanocomposite exchanger may be due to the binding of organic polymeric material with inorganic moiety. This nanocomposite exchanger showed a good reproducible characteristic which is evident from the fact that the material obtained from various batches under identical conditions did not show any appreciable change in the percentage of yield and ion exchange capacity.

Table 2 depicts the effect of temperature on ion exchange capacity of nanocomposite. Ion exchange capacity decreased with increase in temperature. The results revealed that CA/ZPNC possessed high thermal stability as the sample retained about 30% of the initial ion exchange capacity even after heating up to 400 °C.

The effect of eluent concentration on ion exchange capacity of CA/ZPNC was investigated. The rate of elution was governed by the concentration of the eluent and this behaviour is typical of the composite ion exchange materials (Inamuddin et al., 2007; Siddiqui & Khan, 2007). Optimum concentration of $NaNO_3$ as eluent for CA/ZPNC was found to be 1 M for maximum release of H^+ ions.

The elution behaviour of CA/ZPNC confirmed that all the exchangeable H^+ ions were eluted out at 150 mL of the effluent.

pH titration behaviour at equilibrium conditions for CA/ZPNC with NaOH–NaCl system illustrated the mono functional nature of nanocomposite. The CA/ZPNC behaved as a strong cation exchanger as indicated by the low pH of the solution when no OH^- ions were added.

The distribution studies showed that CA/ZPNC exchanger was found to be highly selective for Pb^{2+} and Zn^{2+} as compared to the other metal ions. Thus the composite can be utilized for separation and determination of lead and zinc ions from waste effluents (Siddiqui & Khan, 2007).

Based upon K_d values, the order of selectivity for different metal ion was found as: Pb^{2+} (K_d = 220 mL/g) > Zn^{2+} (K_d = 200 mL/g) > Th^{2+} (K_d = 92 mL/g) > Cu^{2+} (K_d = 62.7 mL/g) > Ni^{2+} (K_d = 62.0 mL/g) > Cd^{2+} (K_d = 60.16 mL/g) > Mg^{2+} (K_d = 40.5 mL/g). The distribution studies showed that CA/ZPNC exchanger was highly selective for Pb^{2+} and Zn^{2+} ions as compared to other metal ions.

3.3. Photocatalytic activity of CA/ZPNC

The photocatalytic activity of CA/ZPNC, ZP (S-1) was evaluated for the degradation of Congo red (CR) dye in the presence of solar light (Fig. 5(a)). The decrease in CR concentration was more with CA/ZPNC which shows that the composite has higher activity as compared to CA and ZP. The direct photolysis in absence of photocatalyst did not show any significant effect on CR degradation. However, CR degradation increased appreciably in the presence of both sunlight and catalyst (CA/ZPNC). When CA/ZPNC was irradiated with solar light, the charge separation produced electron–hole pair (h^-_{vb}/e^+_{CB}). The conduction band electrons were transferred to catalyst surface. The conduction band electrons reduced the O_2 and formed the hydroxyl radicals. The valance band holes acted as the electron sink and reacted with H^+/H_2O at the catalyst surface to form OH radicals (Sillanppa,

Table 1
Synthesis of different samples of cellulose acetate Zr (IV) phosphate nanocomposite (CA/ZPNC) exchanger.

Sample no.	Mixing volume rations of reagents (v/v)			Total volume (mL)	pH	Colour of precipitates	Yield (g)	IEC for Na^+ (meq g^{-1})
	Cellulose acetate in formic acid (%w/v)	Zirconium oxychloride (0.1 M)	Orthophosphoric acid (0.1 M)					
S-1	1	100	50	175	1.0	White	1.91	1.4
S-2	2	100	50	175	1.0	White	2.00	1.1
S-3	3	100	50	175	1.0	White	3.10	0.56
S-4	4	100	50	175	1.0	White	3.76	0.58
S-5	0	100	50	175	1.0	White	3.00	0.5

Table 2
Effect of temperature on ion exchange capacity of cellulose acetate Zr (IV) phosphate nanocomposite (CA/ZPNC) exchanger.

Heating temperature (°C)	Weight before heating	Weight after heating	Colour after heating	IEC for Na^+ ion (meq g^{-1})	Retention of ion exchange capacity
75	0.53	0.48	White	1.3	92.85
100	0.53	0.47	White	1.28	91.42
200	0.53	0.41	Dark brown	0.82	58.57
300	0.53	0.40	Brown	0.64	45.71
400	0.53	0.35	Light brown	0.42	30.00

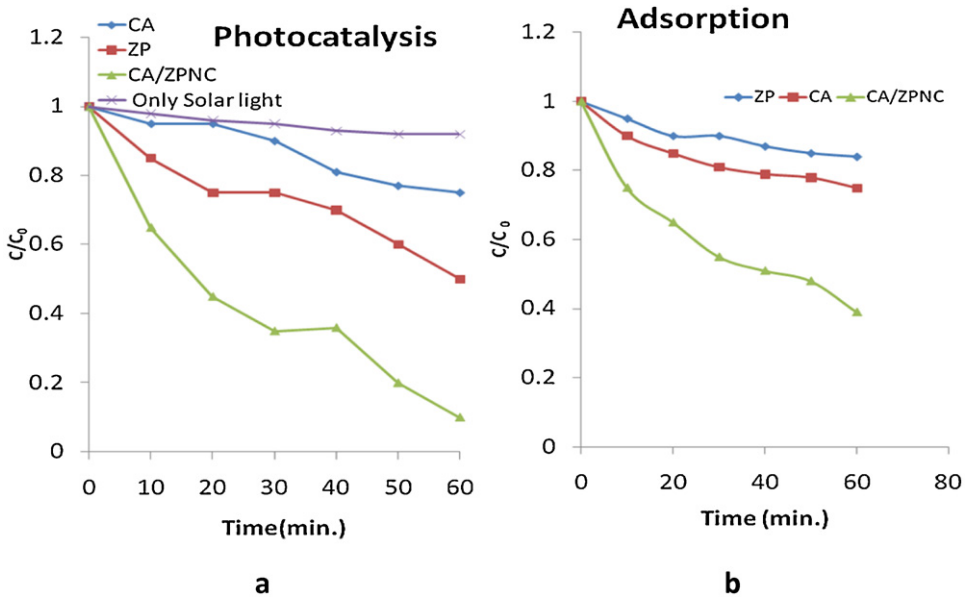

Fig. 5. Photocatalytic degradation (a) and adsorption removal (b) of CR dye under different systems. [CR] = 100 mg/100 mL, pH = 4, catalyst/adsorbent dose = 5 mg/100 mL, time = 60 min and solar intensity = $56 \times 10^4 \pm 250$ lx.

Kurniawasn, & Lo, 2011). The highly oxidizing hydroxyl radicals (redox potential = 2.8 ev) caused the degradation of the CR dye. As shown in Fig. 5(a), 90% of CR was removed in 60 min of irradiation involving pseudo-first-order rate constant ($k_{obs} = 0.0655\ min^{-1}$). However, 40 and 20% of CR removal was observed in the case of ZP ($k_{obs} = 0.0315\ min^{-1}$) and CA ($k_{obs} = 0.015\ min^{-1}$), respectively. In similar studies, Sun, Wang, Sun, and Dong (2009) investigated hydroxyl radical induced degradation of CR using pseudo-first-order kinetics ($k_{obs} = 0.0355\ min^{-1}$). Zhu et al. (2009) reported pseudo-first-order rate constant, $0.011\ min^{-1}$ at pH 6 for photodegradation of CR. Adsorption plays a very crucial role in the photodegradation process and occurs on the surface of nanocomposite. The photodegradation of the dye depends on the concentration of dye in both the bulk solution and on the catalyst surface. The real photodegradation can be explained on the basis of the decrease in the dye concentration both in bulk solution and on the catalyst surface (Zhang et al., 1998; Hu, Tang, Yu, & Wong, 2003). The higher adsorption capacity of CA/ZPNC was due to the presence of both cellulose acetate and ZP in the nanocomposite (Fig. 5(b), Xu, Cai, & Shea, 2007).

In the case of CA/ZPNC, the effect of adsorption in photodegradation of CR was studied under three reaction conditions. The three reaction conditions i.e., equilibrium adsorption in dark, equilibrium adsorption followed by photodegradation, and simultaneous adsorption and degradation are denoted by CA/ZPNC/DA, CA/ZPNC/A – P and CA/ZPNC/A + P, respectively, unless, otherwise specified (Fig. 6). In simultaneous adsorption and degradation process (A + P), 95% of the dye in bulk solution was degraded in 60 min under solar light while in dark adsorption (DA) only 40% of dye was removed. During CA/ZPNC/A – P process, the catalyst particles were highly covered by CR molecules. Such high coverage by CR dye molecules might cut off the sunlight, resulting in lower degradation of CR. In case of simultaneous adsorption and photocatalytic process, the instant amount of dye adsorbed ontoCA/ZPNC at each time was not very high; thereby causing weak screening effect to sunlight and hence to provide adequate active sites for the creation of valence- band holes and conduction band electrons (Gupta et al., 2012a; Xu et al., 2007). On the other

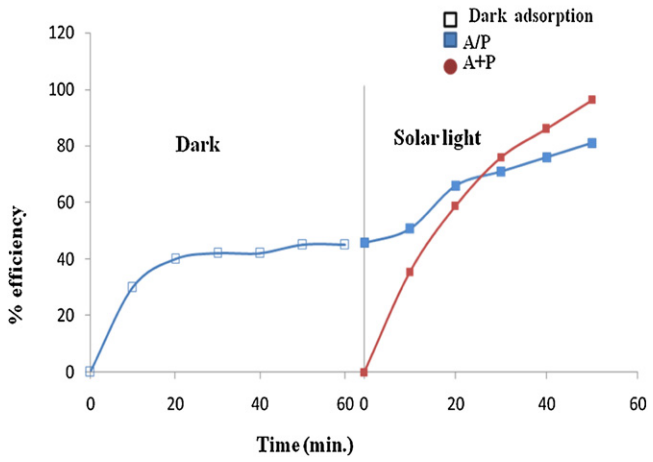

Fig. 6. CR degradation onto CA/ZPNC under different system: [CR] = 100 mg/100 mL, pH = 4, catalyst dose = 5 mg/100 mL, time = 60 min and solar intensity = $56 \times 10^4 \pm 250$ lx.

hand, the adsorbed dye molecules could be degraded rapidly during simultaneous photocatalysis. This concurrent photodegradation increased the sunlight transmittance to catalyst surface and improved the process efficiency.

4. Conclusion

In the present study, an ambient reaction condition method was developed to prepare cellulose acetate–zirconium (IV) phosphate nanocomposite. Spectral analysis confirmed the high level of CA and zirconium (IV) phosphate nanocomposite formation. CA/ZPNC was stable at high temperature exhibiting promising ion exchange capacity and photocatalytic activity. The ion exchange capacity decreased with increase in temperature. CA/ZPNC behaved as strong cation exchanger, showing high selectivity to Pb^{2+}. Congo red dye was successfully degraded in CA/ZPNC/solar light system. The simultaneous adsorption and photocatalysis processes proved to be highly efficient for Congo red dye degradation.

References

Ali, I. (2012). New generation adsorbents for water treatment. *Chemical Reviews*, *112*, 5073–5091.

Chatterjee, S., Lee, D. S., Lee, M. W., & Woo, S. H. (2009). Enhanced adsorption of Congo red from aqueous solutions by chitosan hydrogel beads impregnated with cetyltrimethyl ammonium bromide. *Bioresource Technology*, *100*, 2803–2809.

Constantin, M., Asmarandei, I., Harabagiu, V., Ghimici, L., Ascenzi, P., & Fundueanu, G. (2013). Removal of anionic dyes from aqoueus solutions by an ion-exchanger based on pullulan microsphere. *Carbohydrate Polymers*, *91*, 74–84.

Dong, F., Sun, Y., Min, Fu, Wu, Z., & Lee, S. C. (2012). Room temperature synthesis and highly enhanced photocatalytic activity of porous BiOI/BiOCl composites nanoplates microflowers. *Journal of Hazardous Materials*, *219*, 26–34.

Fitz-Binder, C., & Bechtold, T. (2012). Ca^{2+} sorption on regenerated cellulose fibres. *Carbohydrate Polymers*, *90*, 937–942.

Gupta, V. K., Ali, I., & Saini, V. K. (2007). Defluoridation of wastewaters using waste carbon slurry. *Water Research*, *41*(15), 3307–3316.

Gupta, V. K., Jain, R., & Varshney, S. (2007). Electrochemical removal of the hazardous dye Reactofix Red 3 BFN from industrial effluents. *Journal of Colloid and Interface Science*, *312*, 292–296.

Gupta, V. K., Agarwal, S., & Saleh, T. A. (2011). Chromium removal by combining the magnetic properties of iron oxide with adsorption properties of carbon nanotubes. *Water Research*, *45*, 2207–2212.

Gupta, V. K., Mittal, A., Malviya, A., & Mittal, J. (2009). Adsorption of carmoisine A from wastewater using waste materials-Bottom ash and deoiled soya. *Journal of Colloid and Interface Science*, *335*, 24–33.

Gupta, V. K., Rastogi, A., & Nayak, A. (2010). Biosorption of nickel onto treated alga (Oedogoniumhatei): Application of isotherm and kinetic models. *Journal of Colloid and Interface Science*, *342*(2), 533–539.

Gupta, V. K., Gupta, B., Rastogi, A., Nayak, A., & Agarwal, S. (2011). A comparative investigation on adsorption performances of mesoporous activated carbon prepared from waste rubber tire and activated carbon for a hazardous azo dye-acid blue 113. *Journal of Hazardous Materials*, *186*, 891–901.

Gupta, V. K., Ali, I., Saleh, T. A., Nayak, A., & Agarwal, S. (2012). Chemical treatment technologies for wastewater recycling – A review. *RSC Advances*, *2*, 6380–6388.

Gupta, V. K., Pathania, D., Agarwal, S., & Singh, P. (2012). Preparation of cellulose acetate-zirconium (IV) phosphate nanocomposite with ion exchange capacity and enhanced photocatalytic activity. *Journal of Hazardous Materials*, *243*, 179–186.

Hu, C., Tang, Y. C., Yu, J. C., & Wong, P. K. (2003). Photocatalytic degradation of cationic blue X-GRL adsorbed on TiO_2/SiO_2 photocatalyst. *Applied Catalysis B*, *40*, 131–140.

Huang, S. H., & Chen, D. H. (2009). Rapid removal of heavy metals cations and anions from aqueoussolution by an amino-fucntionalized magnetic nano-adsorbent. *Journal of Hazardous Materials*, *163*, 174–179.

Inamuddin, Khan, S. A., Siddiqui, W. A., & Khan, A. A. (2007). Synthesis, characterization and ion-exchange properties of a new and novel 'organic–inorganic hybrid' cation-exhanger: Nylon-6,6,Zr (IV) phosphate. *Talanta*, *71*, 841–847.

Jain, A. K., Gupta, V. K., Bhatnagar, A., & Suhas. (2003). A comparative study of adsorbents prepared from industrial wastes for removal of dyes. *Separation Science and Technology*, *38*, 463–481.

Jo, W. K., Shin, S. H., & Wang, E. S. H. (2011). Removal of dimethyl sulphide utilizing activated carbon fiber-supported photocatalyst in continuous-flow system. *Journal of Hazardous Materials*, *191*, 234–239.

Korbahti, B. K., Artut, K., Gecgel, C., & Ozer, A. (2011). Electrochemical decolorization of textile dyes and removal of metal ions from textile dye and metal ion binary mixtures. *Chemical Engineering Journal*, *173*, 677–688.

Kubli, T., Sisak, D., Baerlocher, C., McCuser, L. B., Liu, L., Yang, J., et al. (2012). Synthesis, structure, and characterization of ZrPOF-DEA, a mesoprous zirconium Phosphate framework materials. *Microporous and Mesoporous Materials*, *164*, 82–87.

Liu, C., Ma, J., Gan, X., Li, R., & Wang, J. (2012). Effect of chain length of the layered zirconium phosphate on the structure and properties of castor oil-based polyurethane nanocomposites. *Composites Science and Technology*, *72*, 915–923.

Liu, S., Sun, H., Liu, S., & Wang, S. (2013). Graphene facilitated visible light photodegradation of methylene blue over titanium dioxide photocatalysts. *Chemical Engineering Journal*, *214*, 298–303.

Mishima, T., Matsuda, M., & Miyake, M. (2007). Visible-light photocatalytic properties and electronic structure of Zr-based moxynitride, Zr_2ON_2, derived from nitridation of ZrO_2. *Applied Catalysis A: General*, *324*, 77–82.

Mittal, A., Gupta, V. K., Malviya, A., & Mittal, J. (2008). Process development for the batch and bulk removal and recovery of a hazardous, water-soluble azo dye (Metanil Yellow) by adsorption over waste materials (Bottom Ash and De-Oiled Soya). *Journal of Hazardous Materials*, *151*, 821–832.

Mittal, A., Mittal, J., Malviya, A., & Gupta, V. K. (2009). Adsorptive removal of hazardous anionic dye "Congo red" from wastewater using waste materials and recovery by desorption. *Journal of Colloid and Interface Science*, *340*, 16–26.

Mittal, A., Mittal, J., Malviya, A., & Gupta, V. K. (2010). Removal and recovery of Chrysoidine Y from aqueous solutions by waste materials. *Journal of Colloid and Interface Science*, *344*, 497–507.

Mittal, A., Mittal, J., Malviya, A., Kaur, D., & Gupta, V. K. (2010). Adsorption of hazardous dye crystal violet from wastewater by waste materials. *Journal of Colloid and Interface Science*, *343*, 463–473.

Nevarez, L. M., Casarrubias, L. B., Canto, O. S., Celzard, A., Fierro, V., Gomez, R. I., et al. (2011). Biopolymers-based nanocomposites: Membranes from propionated lignin and cellulose for water purification. *Carbohydrate Polymer*, *86*, 732–741.

Oei, B. C., Ibrahim, S., Wang, S., & Ang, H. M. (2009). Surfactant modified barley straw for removal of acid and reactive dyes from aqueous solution. *Bioresource Technology*, *100*, 4292–4295.

Park, B. D., & Kadla, J. F. (2012). Thermal degradation kinetics of resole phenol-formaldehyde resin/multi-walled carbon/cellulose nanocomposite. *Thermochimica Acta*, *540*, 107–115.

Qourzal, S., Tamimi, M., Assabbane, & Ait-Ichou, A. Y. (2005). Photocatalyticdegradationand adsorption of 2-naphthol on suspended TiO_2 surface in a dynamic reactor. *Journal of Colliodal and Interface Science*, *286*, 621–626.

Siddiqui, W. A., Khan, S. A., & Inamuddin. (2007). Synthesis, characterization and ion-exchange properties of a new and novel 'organic–inorganic hybrid' cation-exchanger: Poly(methylene methacrylate) Zr (IV) phosphate. *Colloids and Surfaces A: Physicochemical and Engineering Aspects*, *295*, 193–199.

Sillanppa, M. E. T., Kurniawasn, T. A., & Lo, W. L. (2011). Degradation of chelating agents in aqueous solution using advanced oxidation process (AOP). *Chemosphere*, *83*, 1443–1460.

Sun, J. H., Wang, Y. K., Sun, R. X., & Dong, S. Y. (2009). Photo degradation of azo dye Congo red from aqueous solution by the WO_3–TiO_2/activated carbon (AC) photo catalyst under UV irradiation. *Materials Chemistry and Physics*, *115*, 303–308.

Thakkar, R., & Chudasama, U. (2009). Synthesis and characterization of zirconium titanium phosphate and its application in separation of metal ions. *Journal of Hazardous Materials*, *172*, 129–137.

Vilhera, C., Goncalves, M. L., & Mota, A. M. (2004). Binding of copper(II) to pectin by electromchemical methods. *Electroanalytical*, *16*, 2065–2072.

Virkutyte, J., Jegatheesan, V., & Varma, R. S. (2012). Visible light activated TiO_2/microcrystalline cellulose nanocatalyst to destroy organic contaminant in water. *Bioresource Technology*, *113*, 288–293.

Xu, T. L., Cai, Y. O., & Shea, K. E. (2007). Adsorption and photocatalysed oxidation of methylated arsenic species on TiO_2 suspension. *Environmental Science Technology*, *41*, 5471–5477.

Yang, Z., Chen, S., Hu, W., Yin, N., Zhang, W., Xiang, C., et al. (2012). Flexible Luminescent CdSe/bacterial cellulose nanocomposite membrane. *Carbohydrate Polymers*, *88*, 173–178.

Zhang, L., Zhao, J. C., Shen, T., Hidaka, H., Pelizzetti, E., & Serpone, N. (1998). TiO_2assistedphotodegrdation of organic pollutants II: Adsorption and degradation kinetics of eosin in TiO_2 in dispersion visible light irradiation. *Applied Catalysis B*, *15*, 147–152.

Zhao, Xue-Tao, Zeng, T., Li, Xue-Yan, Hu, Z. J., Gao, Hong-Wen, & Xie, Z. (2012). Modeling and mechanism of the adsorption of copper ion onto natural bamboo sawdust. *Carbohydrate Polymers*, *89*, 185–192.

Zhu, H., Jiang, R., Xiao, L., Chang, Y., Guan, Y., Li, X., et al. (2009). Photocatalytic decolorization and degradation of Congo red on innovative crosslinked chitosan/nano-CdS composite catalyst under visible light irradiation. *Journal of Hazardous Materials*, *169*, 933–940.